IEEE Photonics Journal
An IEEE Photonics Society Publication

Open Access

Si-Rich Si_xC_{1-x} Light-Emitting Diodes With Buried Si Quantum Dots

Volume 4, Number 5, October 2012

Chih-Hsien Cheng
Chung-Lun Wu
Chun-Chieh Chen
Ling-Hsuan Tsai
Yung-Hsiang Lin
Gong-Ru Lin, Senior Member, IEEE

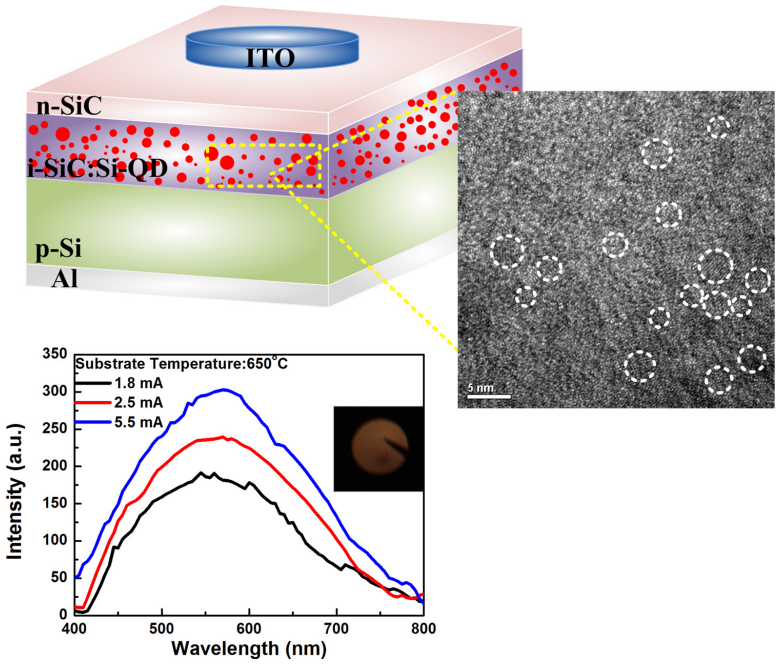

DOI: 10.1109/JPHOT.2012.2215917
1943-0655/$31.00 ©2012 IEEE

Si-Rich Si_XC_{1-X} Light-Emitting Diodes With Buried Si Quantum Dots

Chih-Hsien Cheng, Chung-Lun Wu, Chun-Chieh Chen, Ling-Hsuan Tsai, Yung-Hsiang Lin, and Gong-Ru Lin, *Senior Member, IEEE*

Graduate Institute of Photonics and Optoelectronics, Department of Electrical Engineering, National Taiwan University, Taipei 106, Taiwan

DOI: 10.1109/JPHOT.2012.2215917

Manuscript received July 27, 2012; revised August 19, 2012; accepted August 23, 2012. Date of publication September 4, 2012; date of current version September 8, 2012. This work was supported in part by the National Science Council, Taiwan, and in part by the Excellent Research Projects of the National Taiwan University, Taiwan, under Grants NSC 100-2221-E-002-156-MY3, NSC 101-2622-E-002-009-CC2, NSC 101-ET-E-002-004-ET, and 99R80301. Corresponding author: G.-R. Lin (e-mail: grlin@ntu.edu.tw).

Abstract: The nonstoichiometric ITO/n-SiC/i-SiC/p-Si/Al light-emitting diodes (LEDs) with dense Si quantum dots (Si-QDs) embedded in the Si-rich Si_xC_{1-x}-based i-SiC layer are demonstrated. The Si-rich Si_xC_{1-x} films with buried Si-QDs are grown by the plasma-enhanced chemical vapor deposition with varying substrate temperatures. After the annealing process, the average Si-QD size in the Si-rich $Si_{0.52}C_{0.48}$ film is 2.7 $\pm$ 0.4 nm with a corresponding volume density of 1.43×10^{18} cm^{-3}. By increasing the deposition temperatures from 300 °C to 650 °C, the turn-on voltage and turn-on current of the ITO/n-SiC/i-SiC/p-Si/Al LEDs are found to decrease from 13 to 4.2 V and from 0.63 to 0.34 mA, respectively. In addition, these Si-rich Si_xC_{1-x} LEDs provide the maximal electroluminescent (EL) power intensity increasing from 1.1 to 4.5 $\mu W/cm^2$. The yellow (at 570 nm) EL emission power of the ITO/n-SiC/i-SiC/p-Si/Al LEDs reveals a saturated phenomenon due to the Auger effect. The dissipated energy by the lattice thermal vibration contributes to a decayed EL emission power at higher biased currents. The corresponding power–current slope is observed to enhance from 0.45 to 0.61 $\mu W/A$ with the substrate temperature increasing to 650 °C.

Index Terms: Silicon nanophotonics, quantum dots (QDs) and single molecules, light-emitting diodes (LED).

1. Introduction

The nonstoichiometric amorphous silicon carbide (a-SiC)-based light-emitting diodes (LEDs) were extensively investigated because of the C/Si composition ratio detuned bandgap, the visible photoluminescence (PL) region (410–730 nm), and the controllable n- or p-type doping concentrations in SiC films [1]–[4]. The first report on the electroluminescence (EL) of the p-i-n a-SiC LEDs varying from red to green was observed by Kruangam *et al.* [5]. However, Sel and coworkers pointed out that the stoichiometric a-SiC material deteriorated its conductivity and luminescent properties because a lot of defect states were created in the forbidden bandgap of the host matrix by the sp^3 bond configuration between Si and C with dangling bonds [6], [7]. Therefore, many processes have emerged to overcome the limit on the lighting efficiency of the LED made by the indirect bandgap SiC material. Moreover, Jen and coworkers employed the single- or double-graded-gap p-i-n structure to reduce the notch barriers of the a-SiC LEDs [8], [9]. Furthermore, the quantum-well injection was applied to the intrinsic layer for assisting the carrier injection into i-SiC layer; hence, the EL intensity at shorter wavelengths was enhanced under high electric fields [10]. In addition, the Si quantum dots (Si-QDs) embedded in the host matrices, such as Si-rich SiO_x, SiN_x, and SiO_xN_y

films, are another solution to improve the EL intensity because the Si-QDs act as the radiative recombination centers. This mechanism has emerged as a new approach that is different from the radiative mechanisms occurring at the defect states, which are localized at the surface of the Si core or at the extrinsic centers for the confined electron–hole pairs [11]–[19]. Specially, the PL of the Si-QDs embedded in the Si-rich SiN_x film can be detuned from 550 nm to 375 nm by Rodriguez *et al.* [18]. In addition, Park's group further employed a theoretical formula of $E(\text{eV}) = 1.56 + 2.40/d^2$ to obtain the relationship between the PL peak wavelength and the Si-QD size for Si-QDs embedded in the Si-rich SiN_x film [19]. However, the SiO_x and SiN_x host matrices have higher resistivities to make the carriers hardly injected into Si-QDs. To overcome this, the researches on Si-QDs embedded in versatile semiconductor materials, such as ZnO, SiC, etc., have also been comprehensively investigated in recent years [20]–[27]. PL at 685 nm was also demonstrated with Si-QD embedded in ZnO host matrix by Kuo's group [26]. However, the Si-rich Si_xC_{1-x} host matrix is usually employed in recent work. Specially, Kurokawa and coworkers employed the Si-QD/a-SiC superlattice to study its PL at wavelength ranging from 780 nm to 1170 nm [27]. Recently, there are many reports on using the Si-QD embedded in Si-rich Si_xC_{1-x} for fabricating solar cells. Only few reports were emphasized on the LED application using these Si_xC_{1-x}-based thin films with buried Si-QDs [25]. In this paper, the indium tin oxide (ITO)/n-SiC/i-SiC/p-Si/Al LEDs grown with Si-QDs are demonstrated by using the plasma-enhanced chemical vapor deposition (PECVD) system at different substrate temperatures. The optical and electrical properties of the ITO/n-SiC/i-SiC/p-Si/Al LEDs are discussed.

2. Experimental Details

2.1. Si-QD-Based ITO/n-SiC/i-SiC/p-Si/Al LEDs Fabrication

The 50-nm-thick Si-rich Si_xC_{1-x} films were deposited on a p-type (100)-oriented Si substrate by using the PECVD system at a chamber pressure of 0.3 torr and an RF plasma power of 20 W. The Argon (Ar)-diluted SiH_4 fluence was fixed at 75 sccm with a fluence ratio defined as $R = [CH_4]/([CH_4] + [SiH_4]) \times 100\% = 60\%$. The substrate temperature was varied from 300 °C to 650 °C. Afterwards, the Si-rich Si_xC_{1-x} films were annealed in a quartz furnace at 1100 °C under the Ar atmosphere for 30 min in order to synthesize the Si-QDs. Then, the 25-nm-thick phosphor-doped n-SiC film that served as an ohmic contact was deposited on the Si-rich Si_xC_{1-x} films with buried Si-QDs. A 100-nm-thick ITO film with a diameter of 0.8 mm was deposited on the top of the n-SiC film by e-gun evaporation to form ITO/n-SiC/i-SiC/p-Si/Al LEDs. A 150-nm-thick Al contact electrode was coated at the bottom of the Si substrate by thermal evaporation. Later on, all samples were annealed in a quartz furnace at 450 °C for 30 min to improve the contact resistivity. The Si-QD size in Si-rich Si_xC_{1-x} film was determined by using a high-resolution transmission electron microscopy (HRTEM, JEOL 4000EX) analysis. The current-voltage (I–V) analysis of the ITO/n-SiC/i-SiC/p-Si/Al LEDs was measured by a programmable electrometer (Keithley, model 237). The room-temperature EL spectrum ranging from 400 to 800 nm was measured by using a monochromator (CVI, model DK240), a photomultiplier (Hamamatsu, model R928), and a multimeter (HP, model 34401A). All samples were diced to a suitable size and put into a Si integral sphere head (ILX, model OMH-6703B) in connection with a power multimeter (ILX, model OMM-6810B) for detecting the EL emission power in the continuous-wave (CW) current mode. For the pulsed current operation, the devices were driven by a pulsed current with a duty cycle and a pulsewidth of 1 % and 1 ms, respectively.

3. Results and Discussion

3.1. TEM and XPS of the Si-Rich Si_xC_{1-x} Films With Buried Si-QDs

The cross-sectional bright-field HRTEM images confirm the existence of Si-QDs embedded in the Si-rich Si_xC_{1-x} host matrix after annealing at 1100 °C for 30 min, as shown in Fig. 1(a). The size distribution of Si-QDs in Fig. 1(b) reveals that the Si-QD diameter is ranged between 1.7 and 3.7 nm,

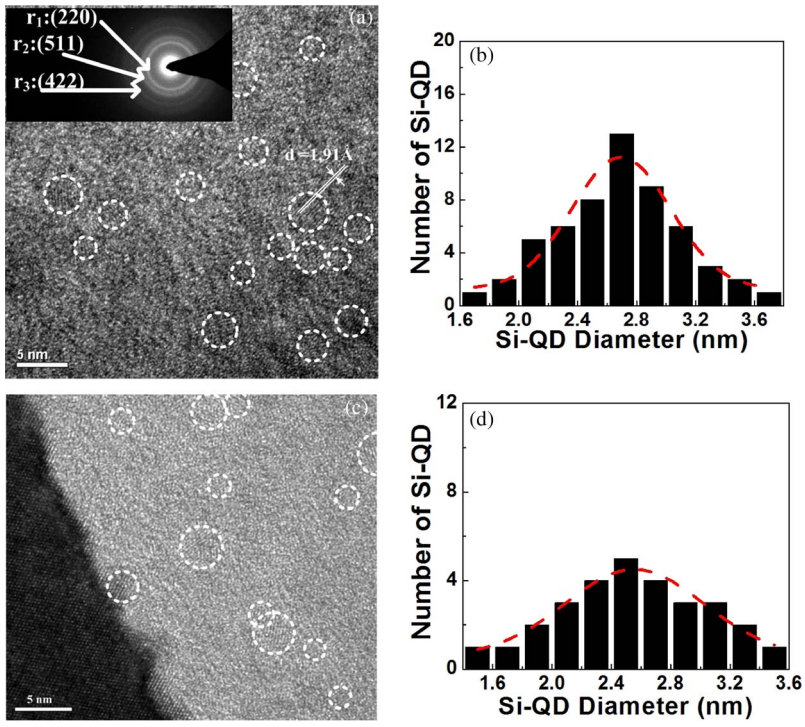

Fig. 1. (a) HRTEM image for the 2.7 ± 0.4 nm large Si-QDs embedded in Si_xC_{1-x} film grown at substrate temperature of 650 °C. (b) Size distribution of Si-QDs embedded in Si_xC_{1-x} film grown at substrate temperature of 650 °C. (c) HRTEM image for the 2.5 ± 0.5 nm large Si-QDs embedded in SiO_x sample grown at substrate temperature of 300 °C. (d) Size distribution of Si-QDs embedded in Si_xC_{1-x} films grown at substrate temperature of 300 °C.

which can be fitted by a Gaussian function with a peak at 2.7 nm and a full-width at half-maximum at 0.8 nm. In Fig. 1(a), the TEM-estimated volume density of Si-QDs in Si-rich Si_xC_{1-x} host matrix is controlled at 1.43×10^{18} cm^{-3}. The size distribution of Si-QDs shown in Fig. 1(d) reveals that the Si-QD diameter is ranged between 1.5 and 3.5 nm, which can be fitted by a Gaussian function with a peak at 2.5 nm and a full-width at half-maximum at 1 nm. The TEM-estimated volume density of Si-QDs in Si-rich Si_xC_{1-x} host matrix is controlled at 7.3×10^{17} cm^{-3}. The Si-QD slightly increases its size in Si-rich Si_xC_{1-x} film grown by decreasing the substrate temperature. For the Si-rich Si_xC_{1-x} grown at higher substrate temperatures, the excessive Si atoms are easily deposited on the substrate because the Si atoms have a faster deposition rate under the higher substrate temperatures [28]. According to the literature, the excessive Si content in a-SiC films is directly proportional to deposition temperature during PECVD growth, as reported by Huran *et al.* [28]. Therefore, the Si-rich Si_xC_{1-x} matrix gradually changes to a highly Si-rich Si_xC_{1-x} structure by increasing the substrate temperature. In our previous work, the C/Si composition ratio of the Si-rich Si_xC_{1-x} film has shown an impact on a formation of the self-aggregate Si-QDs [24]. With a smaller C/Si composition ratio, the excessive Si atoms observed in the Si-rich Si_xC_{1-x} film have larger diffusion coefficients. The larger diffusion coefficient contributes to a longer diffusion length for excessive Si atoms. The longer diffusion length makes the self-aggregated Si-QD larger in Si-rich Si_xC_{1-x} film. In addition, it also contributes to the higher volume density of Si-QDs. Therefore, the Si-rich Si_xC_{1-x} films grown at higher temperature exhibit the larger Si-QDs and the higher volume density. The pattern of the selected area diffraction (SAD) for Si-QDs embedded in Si-rich Si_xC_{1-x} film after annealing at 1100 °C for 30 min is observed, as shown in the inset of Fig. 1(a). The SAD pattern shows the diffraction rings (r_1, r_2, and r_3) for Si-QDs embedded in Si-rich Si_xC_{1-x} film, which is due to the contributions of the (220)-, (422)-, and (511)-oriented Si-QDs with corresponding *d*-spacings of 1.92 Å, 1.37 Å, and 1.10 Å, respectively [29], [30]. Moreover, the

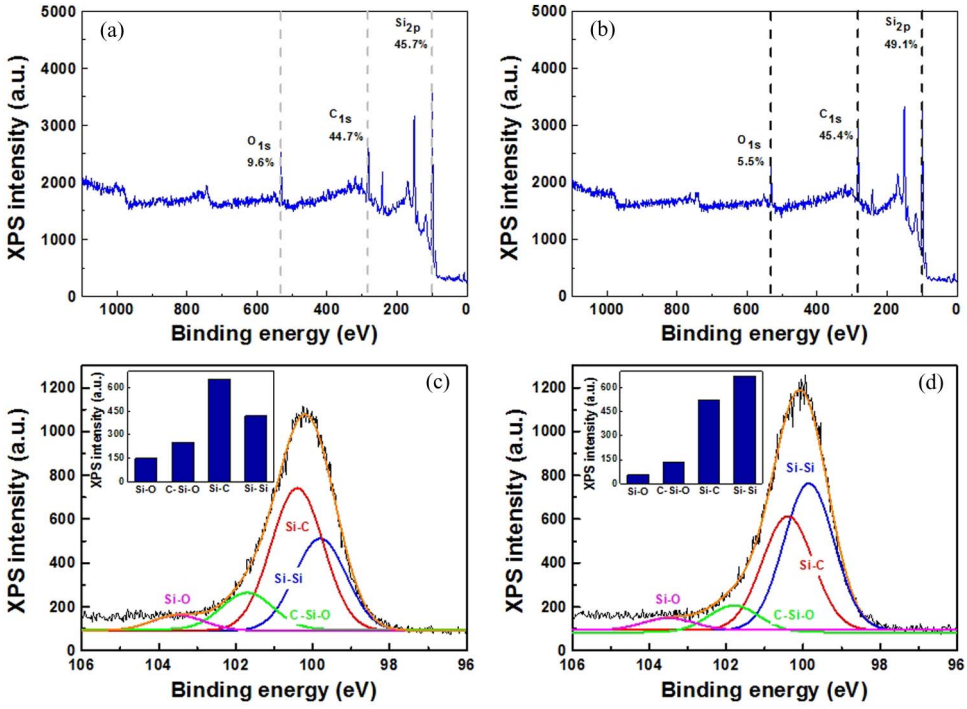

Fig. 2. XPS analysis of Si-rich SixC1-x films with buried Si-QDs grown at substrate temperatures of (a) 300 °C and (b) 650 °C. The $Si_{(2p)}$ related XPS spectra of the Si-rich SixC1-x films with buried Si-QDs grown at substrate temperatures of (c) 300 °C and (d) 650 °C. Inset: The compositional bonds and their dependent XPS intensities within the $Si_{(2p)}$ spectrum.

preferred orientation of the Si-QDs in Si-rich Si_xC_{1-x} films after annealing at 1100 °C is (220), which is confirmed by the corresponding *d*-spacing of 1.91 ± 0.01 Å.

Fig. 2(a) and (b) shows that the composition ratio x of the Si-rich Si_xC_{1-x} films varies from 0.506 to 0.52 owing to the increased Si concentration in Si-rich Si_xC_{1-x} films. The O/Si ratio is reduced from 0.21 to 0.112 by increasing the deposition temperature from 300 °C to 650 °C, which is due to a better crystallinity of PECVD growth Si_xC_{1-x} material so that the oxygen invasion in Si-rich Si_xC_{1-x} films can be prevented. In addition, the oxygen contents in Si-rich Si_xC_{1-x} films are reduced from 300 °C to 650 °C since the oxygen atoms are easily escaped from the Si-rich Si_xC_{1-x} film. In other words, the oxygen atoms are hardly deposited into a-Si_xC_{1-x} films during PECVD growth under the higher temperature. Therefore, the Si-rich Si_xC_{1-x} film grown at higher substrate has the lower oxygen content. By comparing the Si-rich Si_xC_{1-x} film grown at substrate temperatures of 300 °C and 650 °C in Fig. 2(c) and (c), the X-ray photoelectron spectroscopy (XPS) signals indicated a phase change in the Si-rich Si_xC_{1-x} film by fitting the $Si_{(2p)}$ electron related XPS spectra with four separated Gaussian components with their binding energies at 99.7, 100.5, 101.5, and 103.35 eV attributed to the Si–Si bonds, Si–C bonds, C–Si–O bonds, and O–Si–O bonds, respectively. The Si–Si bond related signal significantly enhances when growing the Si-rich Si_xC_{1-x} film at substrate temperature of 650 °C, providing an evidence for more Si-QDs precipitated in Si-rich Si_xC_{1-x} film grown at higher deposition temperatures. On the other hand, a reduction in O–Si–O and C–Si–O related signals reveals that the invaded oxygen content decreases in Si-rich Si_xC_{1-x} film grown at higher substrate temperatures.

3.2. Current–Voltage and Power–Current Analyses of the ITO/n-SiC/i-SiC/p-Si/Al LEDs With Buried Si-QDs

In addition, the *I–V* analyses of the ITO/n-SiC/i-SiC/p-Si/Al LEDs grown at different substrate temperatures are performed. The *I–V* responses of the ITO/n-SiC/i-SiC/p-Si/Al LEDs grown at

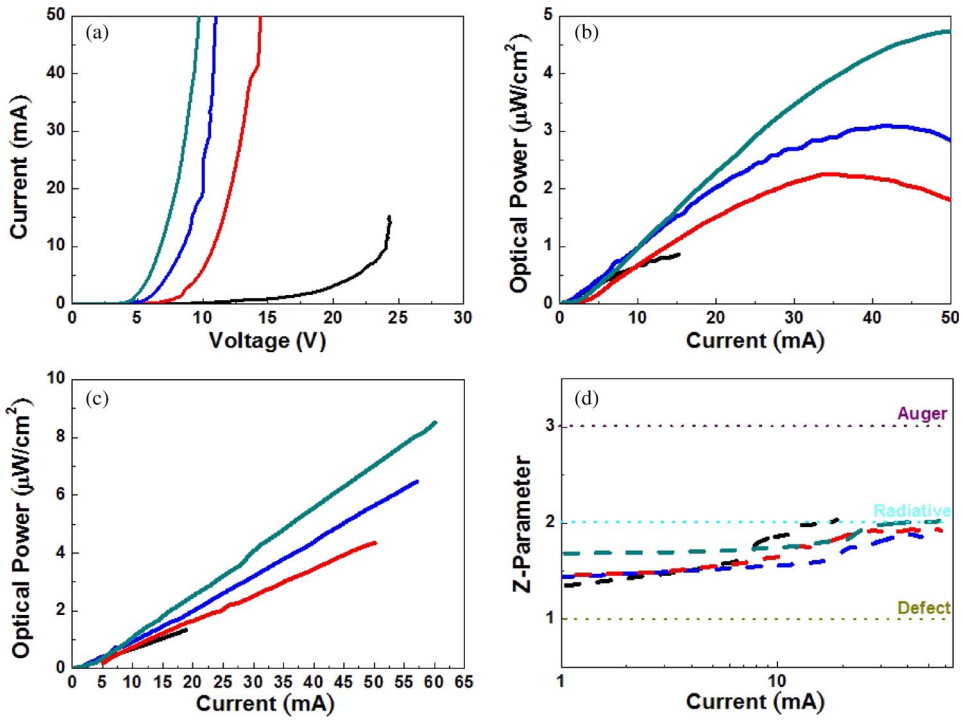

Fig. 3. (a) I–V, (b) P–I curves, and (c) pulsed P–I curves versus biased current of the CW biased ITO/n-SiC/i-SiC/p-Si/Al LEDs grown at substrate temperatures of 300 °C (black), 450 °C (red), 550 °C (blue), and 650 °C (green). (d) The Z-parameter versus biased current of the ITO/n-SiC/i-SiC/p-Si/Al LEDs grown at different substrate temperatures.

different substrate temperatures are shown in Fig. 3(a). Under a forward bias applied from an Al electrode to ITO gate, the electrons and the holes are injected into ITO gate and Si substrate, respectively. Fig. 3(a) illustrates that the corresponding turn-on voltage and the turn-on current of the ITO/n-SiC/i-SiC/p-Si/Al LEDs grown with the substrate temperature increasing from 300 °C to 650 °C are decreased from 13 to 4.2 V and from 0.63 to 0.42 mA, respectively. The Si-rich Si_xC_{1-x} films with buried Si-QDs grown at higher substrate temperatures result in lower C/Si composition ratios, because the Si and C atoms stack much more compact in Si-rich Si_xC_{1-x} film when obtaining a higher thermal energy under the growth at higher substrate temperatures. The turn-on voltage and the turn-on current of the ITO/n-SiC/i-SiC/p-Si/Al LEDs are determined by the resistivity across the Si-rich Si_xC_{1-x} film. The resistivity of the Si-rich Si_xC_{1-x} film with buried Si-QDs is decreased by growing the film at higher substrate temperature, because the high temperature deposition reduces the incorporation of residual oxygen atoms into the as-deposited Si_xC_{1-x} film. In addition, the P–I characteristics of the ITO/n-SiC/i-SiC/p-Si/Al LEDs grown with the substrate temperature increasing from 300 °C to 650 °C indicate that the maximal EL power enhances from 1.1 to 4.5 μW/cm^2 with a corresponding P–I slope increasing from 0.42 to 0.61 μW/A, as shown in Fig. 3(b). In addition, the device could be heated when ITO/n-SiC/i-SiC/p-Si/Al LEDs are CW operated at higher bias currents. This phenomenon contributes to a dramatic degradation on EL power. To avoid the inevitably increased device temperature, the ITO/n-SiC/i-SiC/p-Si/Al LEDs are subsequently biased with a pulsed current. Fig. 3(c) shows the pulsed P–I characteristics of the ITO/n-SiC/i-SiC/p-Si/Al LEDs grown at substrate temperature increasing from 300 °C to 650 °C. The maximal EL power enhances from 1.34 to 8.52 μW/cm^2 with a corresponding P–I slope increasing from 0.44 to 0.75 μW/A. The saturated and degraded phenomenon on the EL power versus current response disappears due to the suppressed heating effect of the device. The controlled device temperature can put off the breakdown of the ITO/n-SiC/i-SiC/p-Si/Al LEDs, which enables the operation at higher biased currents.

In principle, the dominated recombination in a LED can be determined by using the Z-parameter analysis described in [31]. When neglecting the stimulated emission, the net recombination in the steady state is balanced by the injected current as described as

$$I = qV_a(AN + BN^2 + CN^3) \tag{1}$$

where I and V_a are the total current and active volume, respectively. The EL power is proportional to the radiative current (I_{rad}) described as

$$P \propto I_{\text{rad}} \propto N^2. \tag{2}$$

When one of the recombination processes dominates the current, (1) can be approximated by

$$I \propto N^Z. \tag{3}$$

The Z-parameter varies between 1 and 3 for different recombination mechanisms. Typically, the Z-parameters are 1, 2, and 3 for the defect, radiative, and Auger related recombinations, respectively. In the experiment, the Z-parameter can be obtained by plotting the P versus I curve of a LED as the derivative of the $\ln(I)$ versus $\ln(P^{1/2})$ plot. Goddard *et al.* have defined the Z-parameter using the following formula [31]:

$$Z \equiv \frac{d[\ln(I)]}{d[\ln(P^{1/2})]} = 1\frac{I_{\text{defect}}}{I} + 2\frac{I_{\text{rad}}}{I} + 3\frac{I_{\text{Auger}}}{I} \tag{4}$$

where I_{defect}, I_{rad}, and I_{Auger} are the defect, radiative, and Auger currents, respectively. With the Z-parameter experimentally obtained from the pulsed $P-I$ curve, Fig. 3(d) shows the Z-parameter as a function of the pulsed currents for ITO/n-SiC/i-SiC/p-Si/Al LEDs grown at different substrate temperatures. At lower bias currents, the defect and radiative recombinations compete each other in the ITO/n-SiC/i-SiC/p-Si/Al LEDs grown at different substrate temperatures with a corresponding Z-parameter of approximately 1.5. The Z-parameter gradually approaches 2 with increasing biased currents, indicating that the radiative recombination becomes to dominate the ITO/n-SiC/i-SiC/p-Si/Al LEDs under a pulsed bias condition.

In greater detail, the slope of $P-I$ curve is a function of the internal quantum efficiency, which can be derived by the following formula. The rate equation for electron–hole recombination with an external supplied current density of J is described as below

$$\frac{dn(t)}{dt} = \frac{J}{qd} - \frac{n}{\tau} \tag{5}$$

where q is the electron charge, d is the thickness of the recombination region, τ is the carrier lifetime. In equilibrium condition with $dn/dt = 0$, the steady-state current density can be derived as

$$n = \frac{J\tau}{qd}. \tag{6}$$

With the use of (6), the optical power generated internally in the active region of the LED is described as

$$P_{\text{int}} = \eta_{\text{int}}\frac{I}{q}h\nu = \eta_{\text{int}}\frac{hcI}{q\lambda} \tag{7}$$

where P_{int} denotes the optical power, and I the current injected to active region. Therefore, the slope of $P-I$ curve can be described as the following formula:

$$\frac{dP_{\text{int}}}{dI} = \eta_{\text{int}}\frac{hc}{q\lambda}. \tag{8}$$

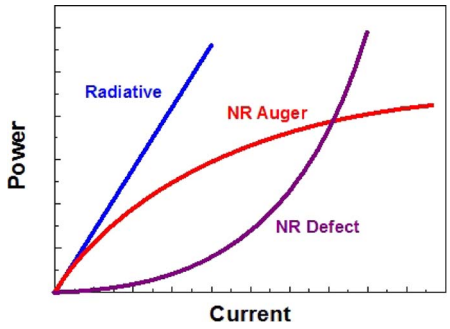

Fig. 4. Power versus current ($P-I$) responses of a LED under the dominated recombination effects by radiative, defect, and Auger, respectively.

In addition, η_{int} is defined as the ratio of radiative recombination rate to the summation of all kinds of recombination rates, as given by

$$\eta_{\text{int}} = \frac{R_{\text{radiative}}}{R_{\text{radiative}} + R_{\text{defect}} + R_{\text{Auger}}} = \frac{R_{\text{radiative}}}{R_{\text{radiative}} + R_{\text{non-radiative}}} = \frac{BN^2}{AN + BN^2 + CN^3} = \frac{\tau_{\text{non-radiative}}}{\tau_{\text{radiative}} + \tau_{\text{non-radiative}}}. \quad (9)$$

That is, the EL power as a function of biased currents can be described as the following formula with the use of (1):

$$P_{\text{int}} = \eta_{\text{int}} \frac{I}{q} h\nu = \eta_{\text{int}} \frac{Ihc}{q\lambda} = \frac{BN^2}{AN + BN^2 + CN^3} \frac{Ihc}{q\lambda} = BN^2 V_a \frac{hc}{\lambda} \quad (10)$$

where N denotes the carrier concentration. In principle, the functions of EL power (P_{EL}) versus biased current (I) can be linear, square, and saturated properties if the recombination is dominated by the defect, radiative, or Auger recombination, respectively. That is, the linear relationship of $P \propto I$ exists only when $I \propto BN^2$ for the radiative dominated recombination, whereas the $P \propto I^2$ shape appears if $I \propto AN$ under the nonradiative defect dominated recombination and the $P \propto I^{2/3}$ shape appears if $I \propto CN^3$ for the Auger dominated recombination. As a result, Fig. 4 illustrates three kinds of $P-I$ responses for a LED dominated by radiative (electron–hole), defect (electron-defect or hole-defect), and Auger (electron–hole–electron, electron–hole–hole, etc.) recombinations, respectively. In our case, the crystallinity of the PECVD-grown SiC material becomes more perfect at higher substrate temperatures, which provides a better band-to-band radiative recombination such that the influence of the Auger effect is postponed to a larger bias condition. The residual oxygen content in Si-rich Si_xC_{1-x} film reduces by increasing the substrate temperature. The reduction of the residual oxygen content in Si-rich Si_xC_{1-x} film contributes to the decreasing resistance in ITO/n-SiC/i-SiC/p-Si/Al LEDs. By $V-I$ analysis, the evaluated resistance of the ITO/n-SiC/i-SiC/p-Si/Al LEDs grown by enlarging the substrate temperature from 300 °C to 650 °C degrades from 1599.6 Ω to 188.5 Ω. The ITO/n-SiC/i-SiC/p-Si/Al LEDs grown at higher substrate temperatures have the larger injection efficiency in active layer due to the decreasing resistance in devices. With the higher injection efficiency, the probability of radiative recombination could be enhanced. The internal quantum efficiency of the ITO/n-SiC/i-SiC/p-Si/Al LEDs increases when enlarging the probability of radiative recombination. Therefore, the ITO/n-SiC/i-SiC/p-Si/Al LEDs grown at higher substrate temperatures have a larger $P-I$ slope.

Except the Auger effect, the thermally assisted carrier leakage could be another possible reason in reducing efficiency at high current density, which is attributed to a small band offset (or effective barrier height) occurred in low-dimensional semiconductor heterostructures. This will lead to an increased thermionic carrier escaping rate [32], [33]. That is because the thermionic carrier escape

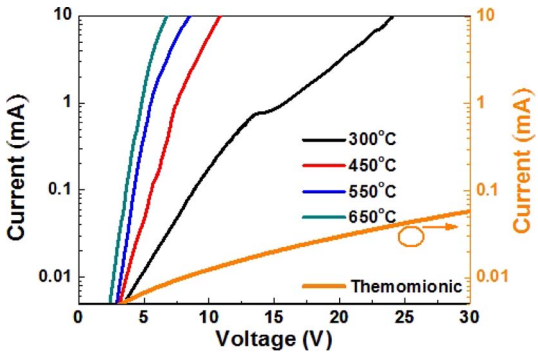

Fig. 5. *I–V* curves of the ITO/n-SiC/i-SiC/p-Si/Al LEDs grown with the different substrate temperatures and the simulated thermionic emission current.

depends on the band offset for both conduction and valence bands. In addition, the thermionic current leakage is described as [32]

$$J = NqLzN_{QD}/\tau \tag{11}$$

where J, N, q, L_z, N_{QD}, and τ are the thermionic leakage current, the number of Si-QDs, the electron charge, the size of Si-QD, the carrier density in Si-QD, and the thermionic carrier escaping time, respectively. With a smaller band offset, it also contributes to a shortened escaping time for thermionic carriers to enhance the thermionic leakage current. Moreover, the current injection efficiency could be determined by [33]

$$\eta_{\text{Injection}} = \left[1 + \frac{\tau_{\text{capture}}}{\tau_B}\left(1 + \frac{\tau_{\text{QD-total}}}{\tau_e}\right)\right]^{-1} \tag{12}$$

where $\eta_{\text{Injection}}$, τ_{capture}, $\tau_{\text{QW-total}}$, and τ_e are the injection efficiency of LEDs, the carrier capture time from the SiC to Si-QD, the carrier recombination lifetime in the Si-QD, the carrier recombination lifetime in SiC, and the carrier escaping time of Si-QD via thermionic emission [33]. The increased thermionic carrier escaping rate at higher current density contributes to the degradation of the injection efficiency and internal quantum efficiency in the active region [32], [33]. The thermionic emission current density is described as [34]

$$J_{\text{thermionic}} = A * T^2 \exp\left(\frac{-q\Phi_B^*}{kT}\right) = A * T^2 \exp\left(\frac{-q}{kT}(\Phi_B - \sqrt{\frac{E_a}{4\pi\varepsilon}}\right) \tag{13}$$

where $A^* = 4\pi qk^2 m^*/h^3 = 120(m^*/m)$, K^2 is Richardson' constant, m is the free electron mass, m^* is the effective mass, Φ_B is the barrier height, E_a is the applied electric field, and T is the absolute temperature. A simulated thermionic current with $m^*/m = 0.33$, $T = 300$ K, and $\Phi_B = 0.6$ eV is shown in Fig. 5, which is much smaller than the real currents obtained from the ITO/n-SiC/i-SiC/p-Si/Al LEDs grown at different substrate temperatures. The thermionic emission process is a minor effect in such ITO/n-SiC/i-SiC/p-Si/Al LEDs. That is, the current transport mechanism is dominated by the F–N tunneling rather than by the thermionic emission.

3.3. Tunneling Mechanism Analysis of the ITO/n-SiC/i-SiC/p-Si/Al LEDs With Buried Si-QDs

Fig. 6(a) shows the band diagram of the ITO/n-SiC/i-SiC/p-Si/Al LEDs without bias. The relationship between the Si-QD size and the luminescent wavelength (bandgap) is described as [35]

$$\lambda = 1.24\left(1.12 + \frac{3.73}{d^{1.39}}\right)^{-1} \tag{14}$$

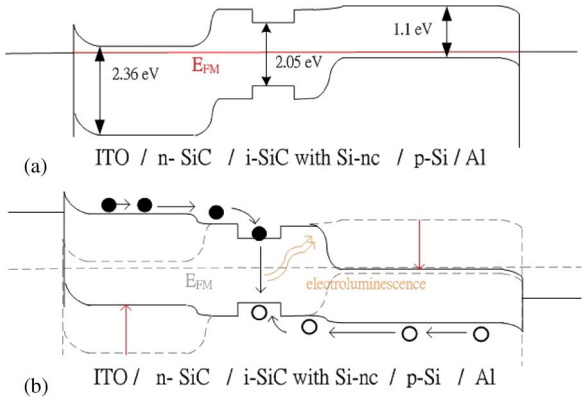

Fig. 6. Band diagram of the ITO/n-SiC/i-SiC/p-Si/Al LEDs (a) without the applied voltage and (b) with applied voltage.

where d and λ are the Si-QD diameter and the luminescent wavelength, respectively. In our case, the Si-QD size at 2.7 $\pm$ 0.4 nm in Si-rich Si_xC_{1-x} film contributes to an EL wavelength of 602 nm (2.05 eV). In addition, Fig. 6(b) shows the band diagram of the ITO/n-SiC/i-SiC/p-Si/Al LEDs with applying bias voltage. The Si-QDs are regarded as the QW to confine the carriers and to generate the EL, because the bandgap energy of the Si-rich Si_xC_{1-x} film is 2.36 eV. Typically, the carriers obtain sufficient energies to easily escape from Si-QDs due to a lower barrier height at the Si-QD/Si_xC_{1-x} interface. The wave function for electrons and holes in Si-QDs will overlap to enhance a probability of the nonphonon assisted recombination. The tunneling probability of the carriers between the Si-QDs for the square potential well is given by:

$$T_e = 16\exp\left\{-d\sqrt{\frac{8m*\Delta E}{\hbar^2}}\right\} \tag{15}$$

where m^*, d, and ΔE are the effective mass of the host matrix, the spacing among Si-QDs, and the energy barrier at SiC/Si-QD interface, respectively. Because the carrier tunneling probability among Si-QDs mainly depends on the barrier height of the host matrix, the quantum confinement effect for Si-QDs embedded in Si-rich Si_xC_{1-x} films thus becomes weaker than that for the Si-QDs embedded in Si-rich SiO_x or SiN_x films [36]–[39]. Due to the higher band energies of the SiO_2 ($\sim$9 eV) and the Si_3N_4 ($\sim$5.3 eV) matrices, the barrier heights at the Si-QDs/SiO_x or the Si-QDs/SiN_x interfaces are much larger than that at the Si-QD/Si_xC_{1-x} interface. Therefore, the tunneling current of the Si_xC_{1-x}-based LEDs is larger than those of the SiO_x- and the SiN_x-based LEDs as the weaker quantum confinement for Si-QDs embedded in Si-rich Si_xC_{1-x} film decreases, thus providing a lower probability of the carrier storage and the electron–hole recombination in Si-QDs embedded in the Si-rich Si_xC_{1-x} films.

In previous works, the Si-rich SiO_x [40]–[42] and SiN_x [16], [37], [43] films are used as host matrices to confine carriers in Si-QDs. However, the SiO_x and SiN_x films are dielectric materials. They contribute to an enhanced resistivity in LEDs to make carriers hardly be injected into Si-QDs without the use of surface roughened nano-structures [44]. The device configuration changes from a MOS to a p-i-n structure when the Si-rich Si_xC_{1-x} film replaces SiO_x or SiN_x films to be employed as a host matrix; the resistivity of the ITO/n-SiC/i-SiC/p-Si/Al LEDs could be significant decreased due to the semiconducting characterization of the Si-rich SiC material. This configuration could lead to an increased injection efficiency to further improve the quantum efficiency of the ITO/n-SiC/i-SiC/p-Si/Al LEDs. In our case, the SiC-based LEDs obtain the lower quantum efficiency due to an invasion of the residual oxygen atoms in Si-rich SiC film during the PECVD and postannealing processes. The invasion of the residual oxygen contributes to additional SiO_x molecules formed in SiC film. These additional SiO_x molecules inevitably increase the resistivity of the SiC film. Therefore, the injection efficiency of the ITO/n-SiC/i-SiC/p-Si/Al LEDs could be degraded due to the

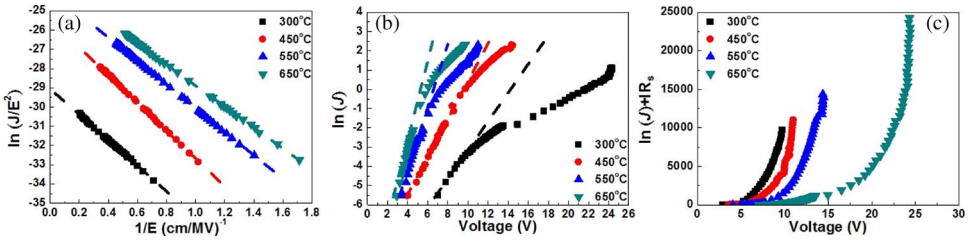

Fig. 7. (a) F–N, (b) the p-n junction and (c) the p-i-n tunneling plots of the ITO/n-SiC/i-SiC/p-Si/Al LEDs grown at different substrate temperatures.

increased resistivity of the Si-rich SiC film. In addition, the doping concentration for n-type SiC film is limited by PECVD growth in our case. The resistivity of the ITO/n-SiC/i-SiC/p-Si/Al LEDs is also enlarged by decreasing the doping concentration for n-type SiC film. Therefore, the external quantum efficiency of the ITO/n-SiC/i-SiC/p-Si/Al LEDs could be further increased by further increasing the doping concentration for n-type SiC film and decreasing the invasion of residual oxygen to enhance the injection efficiency.

The carrier transport mechanism of the F–N tunneling could be considered in our case because the F–N tunneling occurs at high biased field when the metal/Si_xC_{1-x} barrier has a triangular shape for carriers tunneling through only a part of the Si_xC_{1-x} layer. After tunneling through this triangular barrier, the rest of the Si_xC_{1-x} film does not impede the current flow. In other words, the carrier transport is mainly due to the F–N tunneling mechanisms as described by

$$J_{F-N} = \frac{q^3(m_0/m_{ox})}{8\pi h\phi_B}E^2\exp\left(-\frac{8\pi\sqrt{2m_{ox}\phi_B^3}}{3qhE}\right)$$
$$= 1.54\times10^{-6}\frac{(m_0/m_{SiC})}{\phi_B}E^2\exp\left(-6.83\times10^7\frac{\sqrt{(m_{SiC}/m_0)/\phi_B^3}}{E}\right) \quad (16)$$

where q, h, E, m_{ox}, m_0, and F_B are the electron charge, the Planck's constant, the applied electric field, the effective electron mass in the S_xC_{1-x} film, the free electron mass, and the effective barrier height. By linearly fitting the F–N plot of $\ln(J/E^2)$ versus $1/E$ for each ITO/n-SiC/i-SiC/p-Si/Al LEDs, the F–N tunneling behavior can be confirmed according to a observation on the linear turn-on characteristic in the Arrhenius F–N plot, as shown in Fig. 7(a). By increasing the deposition temperature, the increasing turn-on electric field accompanied with interfacial barrier height enlarged from 0.25 to 0.32 eV is observed. The existence of the embedded Si-QDs leads to a decreased turn-on voltage of the F–N tunneling and creates a tunneling path for carriers from Si substrate to ITO contact. The growth at higher deposition temperature suppresses Si-rich condition to shrink the Si-QDs in a more stoichiometric Si_xC_{1-x} film, thus providing a larger interfacial barrier height for carrier tunneling from ITO to Si_xC_{1-x} film.

In addition, the possibility of other tunneling mechanisms for the p-n junction and p-i-n junction should also be considered. The two remarkable tunneling mechanisms are described as below

$$J = J_s\left[\exp\left(\frac{qV}{kT}\right)-1\right] \quad (17)$$

$$J = J_s\left[\exp\left(\frac{q(V-IR_s)}{nkT}\right)-1\right] \quad (18)$$

where J, I, V, and R_s are the current density, the current, the voltage, and the series resistance for ITO/n-SiC/i-SiC/p-Si/Al LEDs, respectively. J_s, k, q, and T are the saturation current density, the Boltzmann constant, the electron charge and the temperature, respectively. Equations (12) and (13) stand for the tunneling mechanism of the p-n and p-i-n junctions, respectively. By linearly fitting the

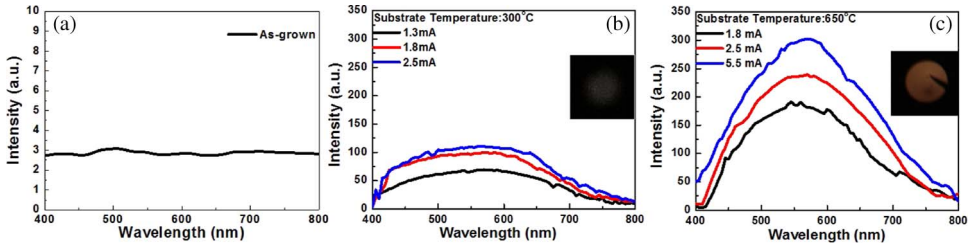

Fig. 8. (a) The EL spectrum of the ITO/n-SiC/i-SiC/p-Si/Al LEDs without Si-QDs. The EL spectra of the ITO/n-SiC/i-SiC/p-Si/Al LEDs grown at substrate temperature of (b) 300 °C and (c) 650 °C with the inset of EL emission pattern.

$\ln(J)$ and $\ln(J) + IR_s$ as a function of V for the ITO/n-SiC/i-SiC/p-SiC/Al LEDs grown at different deposition temperatures, the tunneling behavior could be observed, as shown in Fig. 7(b). Comparing with the aforementioned three tunneling mechanisms, the carrier tunneling in the ITO/n-SiC/i-SiC/p-SiC/Al LEDs is dominated by the F–N tunneling.

3.4. EL Spectrum and Power Analyses of ITO/n-SiC/i-SiC/p-Si/Al LEDs With Buried Si-QDs

The ITO/n-SiC/i-SiC/p-Si/Al LEDs without Si-QDs reveal unobvious EL signals, as shown in Fig. 8(a). The EL of the ITO/n-SiC/i-SiC/p-Si/Al LEDs with Si-QDs is corroborated to the contribution of the buried Si-QDs. The EL spectra of the ITO/n-SiC/i-SiC/p-Si/Al LEDs grown at substrate temperatures of 300 °C and 650 °C are performed and shown in Fig. 8(b) and (b). The EL peak wavelengths of the ITO/n-SiC/i-SiC/p-Si/Al LEDs grown at substrate temperatures of 300 °C and 650 °C are 550 nm and 570 nm, respectively. In addition, the EL peak wavelength of the devices grown at lower substrate temperature is blue-shifted because the Si-QDs embedded in Si-rich Si_xC_{1-x} film have a smaller size distribution. The EL emission patterns of the ITO/n-SiC/i-SiC/p-Si/Al LEDs grown at substrate temperatures of 300 °C and 650 °C under a biased current of 2.5 mA changes from white to yellow, as shown in the inset of Fig. 8(c). The relatively broadened EL spectrum is observed for the ITO/n-SiC/i-SiC/p-Si/Al LED grown at substrate temperature of 300 °C, which is mainly attributed to the broadened size distribution of Si-QDs. As a result, the ITO/n-SiC/i-SiC/p-Si/Al LEDs grown at lower substrate temperatures easily generate a nearly white-light EL pattern as compared with other samples.

Under the higher electric field, the electrons can obtain a larger amount of kinetic energy. That energy can be released through a collision event within the matrix, and the additional electron–hole pair is created in such a manner. The new generated electron–hole pair repeats this mechanism to form other electron–hole pairs. Therefore, numerous electron–hole pairs are created by such an impact ionization procedure, which also affect the EL response. The EL power versus the applied voltage corresponding to the expression for electron accelerated process is described as [45]

$$P = P_0 \exp\left(-\left(\frac{V_0}{V}\right)^{1/2}\right) \tag{19}$$

where P, P_0, V_0, and V are the EL power, the saturation EL power, the saturation voltage, and voltage.

By linearly fitting the $\ln(P)$ versus $V^{-1/2}$ for each ITO/n-SiC/i-SiC/p-Si/Al LEDs, the impact ionization mechanism can be considered according to the observation on the linear fit of the turn-on characteristic, as shown in Fig. 9. With the fitting, the linearly fitted turn-on characteristics appear at higher bias voltages. Therefore, the mechanism of the impact ionization should be considered in our case. The turn-on voltage of the ITO/n-SiC/i-SiC/p-Si/Al LEDs by the impact ionization tunneling decreases from 13.7 V to 7.3 V by increasing the substrate temperature due to the larger C/Si composition ratios and the more residual oxygen content in Si-rich Si_xC_{1-x} film. These phenomena

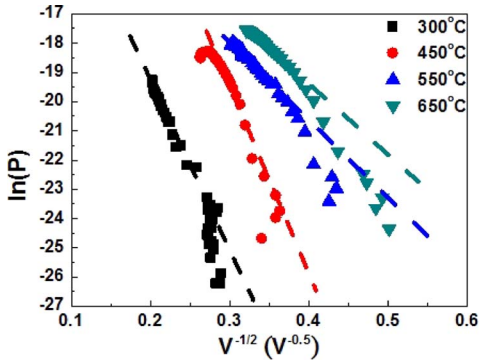

Fig. 9. EL power versus $(\text{voltage})^{-1/2}$ plots of the ITO/n-SiC/i-SiC/p-Si/Al LEDs grown at different substrate temperatures varied from 300 °C to 650 °C.

contribute to the increased bandgap of the Si-rich Si_xC_{1-x} film. The larger bandgap of the Si-rich Si_xC_{1-x} film results in the requirement of a higher electric field to obtain the same impact ionization rate. Therefore, the ITO/n-SiC/i-SiC/p-SiC/Al LEDs grown at lower substrate temperatures need the higher voltage to turn-on the impact ionization tunneling. In addition, the residual oxygen contributes to an additional resistance in ITO/n-SiC/i-SiC/p-Si/Al LEDs to turn-on under the higher electric field. In addition, the mainly dominated tunneling mechanism for the ITO/n-SiC/i-SiC/p-SiC/Al LEDs in our case is F–N tunneling as confirmed by the Arrhenius F–N plot.

4. Conclusion

The Si-QD-based ITO/n-SiC/i-SiC/p-Si/Al LEDs grown at different substrate temperatures have been demonstrated. The HRTEM analysis reveals that the Si-QDs exhibit a size distribution of 2.7 ± 0.4 nm and a volume density of 1.43×10^{18} cm^{-3} in the Si-rich Si_xC_{1-x} film grown at substrate temperature of 650 °C. The turn-on voltage decreases from 13 to 4.2 V by increasing the substrate temperature from 300 °C to 650 °C due to the reducing resistivity of the Si-rich Si_xC_{1-x} host matrix. Concurrently, the turn-on current also decreases from 0.63 to 0.43 mA. Under the growth at higher substrate temperatures, the Si-rich Si_xC_{1-x} film with buried Si-QDs has a lower C/Si composition ratio with reduced oxygen incorporation. By enlarging the substrate temperature, the maximal EL power of the ITO/n-SiC/i-SiC/p-Si/Al LED enhances 1.1 to 4.5 $\mu W/cm^2$ with its corresponding $P-I$ slope increasing from 0.42 to 0.61 $\mu W/A$. The EL power under higher bias currents saturate due to the Auger effect. It starts to decay because the energy is dissipated through the thermal vibration of lattice. The F–N tunneling is the dominated carrier transport mechanism in the ITO/n-SiC/i-SiC/p-Si/Al LEDs. The yellow-emission EL peak wavelength is located at 570 nm for the ITO/n-SiC/i-SiC/p-Si/Al LEDs in Si-rich Si_xC_{1-x} film with a lower C/Si composition ratio grown at higher substrate temperatures.

References

[1] Y. Tawada, M. Kondo, H. Okamoto, and Y. Hamakaw, "Hydrogenated amorphous silicon carbide as a window material for high efficiency a-Si solar cells," *Sol. Energy Mater.*, vol. 6, no. 3, pp. 299–315, Mar./Apr. 1982.
[2] D. Kruangam, T. Endo, P. G. Wei, H. Okamoto, and Y. Hamakawa, "Visible-light injection-electroluminescent a-SiC/p-i-n diode," *Jpn. J. Appl. Phys.*, vol. 24, no. 10, pp. L806–L808, Oct. 1985.
[3] J. Bullot and M. P. Schmidt, "Physics of amorphous silicon–carbon alloys," *Phys. Stat. Sol. (B)*, vol. 143, no. 2, pp. 345–418, Oct. 1987.
[4] D. Kruangam, *Amorphous and Microcrystalline Semiconductor Devices*, J. Kanicki, Ed. London, U.K.: Artech House, 1991.
[5] D. Kruangam, T. Endo, P. G. Wei, S. Nonomura, H. Okamoto, and Y. Hamakawa, "A study of visible-light injection-electroluminescence in a-SiC/p-i-n diode," *J. Non-Cryst. Solids*, vol. 77/78, no. 2, pp. 1429–1432, Dec. 1985.
[6] K. Sel, B. Akaoglu, O. Ozdemir, and I. Atilgan, "Electroluminescence properties of a PIN structure made by nearly stoichiometrica-SiC_x:H active layer," *Vacuum*, vol. 83, no. 5, pp. 813–818, Jan. 2009.

[7] J. Robertson, "The electronic and atomic structure of hydrogenated amorphous Si–C alloys," *Philos. Mag. B*, vol. 66, no. 5, pp. 615–638, Aug. 1992.
[8] J. W. Hong, N. F. Shin, T. S. Jen, S. L. Ning, and C. Y. Chang, "Graded-gap a-SiC:H p-i-n thin-film light-emitting diodes," *IEEE Electron Device Lett.*, vol. 13, no. 7, pp. 375–377, Jul. 1992.
[9] T. S. Jen, N. F. Shin, L. H. Laih, Y. A. Chen, J. W. Hong, and C. Y. Chang, "Electrical and luminescent characteristics of α-SiC:H p-i-n thin-film LED's with graded-gap junctions," *IEEE Trans. Electron Devices*, vol. 44, no. 4, pp. 565–571, Apr. 1997.
[10] T. S. Jen, N. F. Shin, W. C. Tsay, J. Y. Chen, S. L. Ning, J. W. Hong, and C. Y. Chang, "Electroluminescence of a-SiC:H *p-i-n* thin-film light-emitting diodes with quantum-well-injection structures," *Solid State Electron.*, vol. 37, no. 9, pp. 1619–1626, Sep. 1994.
[11] G.-R. Lin and C.-J. Lin, "A CO_2 laser rapid-thermal-annealing SiO_x based metal–oxide–semiconductor light emitting diode," *Appl. Phys. Lett.*, vol. 91, no. 7, pp. 072103-1–072103-3, Aug. 2007.
[12] S. M. Prokes, "Light emission in thermally oxidized porous silicon: Evidence for oxide-related luminescence," *Appl. Phys. Lett.*, vol. 62, no. 25, pp. 3244–3246, Jun. 1993.
[13] S. Fujita and N. Sugiyama, "Visible light-emitting devices with Schottky contacts on an ultrathin amorphous silicon layer containing silicon nanocrystals," *Appl. Phys. Lett.*, vol. 74, no. 2, pp. 308–310, Jan. 1999.
[14] P. Photopoulos and A. G. Nassiopoulou, "Room- and low-temperature voltage tunable electroluminescence from a single layer of silicon quantum dots in between two thin SiO_2 layers," *Appl. Phys. Lett.*, vol. 77, no. 12, pp. 1816–1818, Sep. 2000.
[15] T. W. Kim, C. H. Cho, B. H. Kim, and S. J. Park, "Quantum confinement effect in crystalline silicon quantum dots in silicon nitride grown using SiH_4 and NH_3," *Appl. Phys. Lett.*, vol. 88, no. 12, pp. 123102-1–123102-3, Mar. 2006.
[16] G.-R. Lin, Y.-H. Pai, C.-T. Lin, and C.-C. Chen, "Comparison on the electroluminescence of Si-rich SiN_x and SiO_x based light-emitting diodes," *Appl. Phys. Lett.*, vol. 97, no. 26, pp. 263514-1–263514-3, Jul. 2010.
[17] D. Kruangam, T. Toyama, Y. Hattori, M. Deguchi, H. Okamoto, and Y. Hamakawa, "Valency control of P-type a-SiC:H having the optical band gap more than 2.5 eV by electron-cyclotron resonance CVD (ECR CVD)," *J. Non-Cryst. Solids*, vol. 97/98, no. 2, pp. 1079–1082, Dec. 1987.
[18] A. Rodriguez, J. Arenas, and J. C. Alonso, "Photoluminescence mechanisms in silicon quantum dots embedded in nanometric chlorinated-silicon nitride films," *J. Lumin.*, vol. 132, no. 9, pp. 2385–2389, Sep. 2012.
[19] N.-M. Park, C.-J. Choi, T.-Y. Seong, and S.-J. Park, "Quantum confinement in amorphous silicon quantum dots embedded in silicon nitride," *Phys. Rev. Lett.*, vol. 86, no. 7, pp. 1355–1357, Feb. 2001.
[20] D. Song, E. C. Cho, G. Conibeer, Y. H. Cho, Y. Huang, S. Huang, C. Flynn, and M. A. Green, "Fabrication and characterization of Si nanocrystals in SiC matrix produced by magnetron cosputtering," *J. Vac. Sci. Technol. B, Microelectron. Nanometer Struct.*, vol. 25, no. 4, pp. 1327–1335, Jul. 2007.
[21] Y. Kurokawa, S. Miyajima, A. Yamada, and M. Konagal, "Preparation of nanocrystalline silicon in amorphous silicon carbide matrix," *Jpn. J. Appl. Phys.*, vol. 45, no. 37–41, pp. L104–L1066, Oct. 2006.
[22] D. Song, E. C. Cho, G. Conibeer, C. Flynn, Y. Huang, and M. A. Green, "Structural, electrical and photovoltaic characterization of Si nanocrystals embedded SiC matrix and Si nanocrystals/c-Si heterojunction devices," *Sol. Energy Mater. Sol. Cells*, vol. 92, no. 4, pp. 474–481, Apr. 2008.
[23] C. W. Jianga and M. A. Green, "Silicon quantum dot superlattices: Modeling of energy bands, densities of states, and mobilities for silicon tandem solar cell applications," *J. Appl. Phys.*, vol. 99, no. 11, pp. 114902-1–114902-7, Jun. 2006.
[24] G.-R. Lin, T.-C. Lo, L.-H. Tsai, Y.-H. Pai, C.-H. Cheng, C.-I. Wu, and P.-S. Wang, "Finite silicon atom diffusion induced size limitation on self-assembled silicon quantum dots in silicon-rich silicon carbide," *J. Electrochem. Soc.*, vol. 159, no. 2, pp. K35–K41, Dec. 2011.
[25] Y. Rui, S. Li, J. Xu, C. Song, X. Jiang, W. Li, K. Chen, Q. Wang, and Y. Zuo, "Size-dependent electroluminescence from Si quantum dots embedded in amorphous SiC matrix," *J. Appl. Phys.*, vol. 110, no. 6, pp. 064322-1–064322-6, Sep. 2011.
[26] K.-Y. Kuo, S.-W. Hsu, P.-R. Huang, W.-L. Chuang, C.-C. Liu, and P.-T. Lee, "Optical properties and sub-bandgap formation of nano-crystalline Si quantum dots embedded ZnO thin film," *Opt. Exp.*, vol. 20, no. 10, pp. 104 70–104 75, May 2012.
[27] Y. Kurokawa, S. Tomita, S. Miyajima, A. Yamada, and M. Konagai, "Photoluminescence from silicon quantum dots in Si quantum dots/amorphous SiC superlattice," *Jpn. J. Appl. Phys.*, vol. 46, no. 35, pp. L833–L835, 2007.
[28] Y. J. Huran, B. Zatko, I. Hotovy, J. Pezoldt, A. P. Kobzev, and N. I. Balalykin, "PECVD silicon carbide deposited at different temperature," *Czech. J. Phys.*, vol. 56, pp. B12 07–B12 11, Sep. 2006.
[29] F. L. Normand, J. C. Arnault, S. Pecoraro, and J. Werckmann, "Formation ofβ-SiC nanocrystals on Si(1 1 1) mono-crystal during the HFCVD of diamond," *Appl. Surf. Sci.*, vol. 177, no. 4, pp. 298–302, Jun. 2001.
[30] Y. X. Zhao, F. Buehler, J. R. Sites, and I. L. Spain, "New metastable phases of silicon," *Solid State Commun.*, vol. 59, no. 10, pp. 679–682, Sep. 1986.
[31] L. L. Goddard, S. R. Bank, M. A. Wistey, H. B. Yuen, Z. Rao, and J. S. Harris, Jr., "Recombination, gain, band structure, efficiency, and reliability of 1.5-μm GaInNAsSb/GaAs lasers," *J. Appl. Phys.*, vol. 97, no. 8, pp. 083101-1–083101-15, Apr. 2005.
[32] N. Tansu and L. J. Mawst, "Current injection efficiency of InGaAsN quantum-well lasers," *J. Appl. Phys.*, vol. 97, no. 5, pp. 054502-1–054502-18, Mar. 2005.
[33] H. Zhao, G. Liu, R. A. Arif, and N. Tansu, "Current injection efficiency induced efficiency-droop in InGaN quantum well light-emitting diodes," *Solid State Electron.*, vol. 54, no. 10, pp. 1119–1124, Oct. 2010.
[34] W. Chen, B. Li, H. He, J. Wang, H. L. Tam, K. W. Cheah, X. Cao, Y. Wang, G. Lian, and G. Xiong, "The formation of a charge layer at the interface of GaMnAs and an organic material," *Europhys. Lett.*, vol. 88, no. 4, p. 46002, Nov. 2009.
[35] C. Delerue, G. Allan, and M. Lannoo, "Theoretical aspects of the luminescence of porous silicon," *Phys. Rev. B*, vol. 48, no. 15, pp. 110 24–110 36, Oct. 1993.

[36] G.-R. Lin, C.-J. Lin, and H.-C. Kuo, "Improving carrier transport and light emission in a silicon-nanocrystal based MOS light-emitting diode on silicon nanopillar array," *Appl. Phys. Lett.*, vol. 91, no. 9, pp. 093122-1–093122-3, Aug. 2007.
[37] C.-D. Lin, C.-H. Cheng, Y.-H. Lin, C.-L. Wu, Y.-H. Pai, and G.-R. Lin, "Comparing retention and recombination of electrically injected carriers in Si quantum dots embedded in Si-rich SiN_x films," *Appl. Phys. Lett.*, vol. 99, no. 24, pp. 243501-1–243501-3, Dec. 2011.
[38] G.-R. Lin, C.-J. Lin, and C.-K. Lin, "Enhanced Fowler–Nordheim tunneling effect in nanocrystallite Si based LED with interfacial Si nano-pyramids," *Opt. Exp.*, vol. 15, no. 5, pp. 2555–2563, Mar. 2007.
[39] G.-R. Lin, Y.-H. Pai, and C.-T. Lin, "Microwatt MOSLED using SiO_x with buried Si nanocrystals on Si nano-pillar array," *J. Lightwave Technol.*, vol. 26, no. 11, pp. 1486–1491, Jun. 2008.
[40] G.-R. Lin, C.-J. Lin, C.-K. Lin, L.J. Chou, and Y.-L. Chueh, "Oxygen defect and Si nanocrystal dependent white-light and near-infrared electroluminescence of Si-implanted and plasma-enhanced chemical-vapor deposition-grown Si-rich SiO_2," *J. Appl. Phys.*, vol. 97, no. 9, pp. 094306-1–094306-9, May 2005.
[41] C.-J. Lin and G.-R. Lin, "Defect-enhanced visible electroluminescence of multi-energv silicon-implanted silicon dioxide film," *IEEE J. Quantum Electron.*, vol. 41, no. 3, pp. 441–447, Mar. 2005.
[42] G.-R. Lin, C. J. Lin, and K.-C. Yu, "Time-resolved photoluminescence and capacitance-voltage analysis of the neutral vacancy defect in silicon implanted SiO_2 on silicon substrate," *J. Appl. Phys.*, vol. 96, no. 5, pp. 3025–3027, Sep. 2004.
[43] G.-R. Lin and C.-J. Lin, "Improved blue-green electroluminescence of metal-oxide-semiconductor diode fabricated on multirecipe Si-implanted and annealed SiO_2/Si substrate," *J. Appl. Phys.*, vol. 95, no. 12, pp. 8484–8486, Jun. 2004.
[44] G.-R. Lin, C.-K. Lin, L.-J. Chou, and Y.-L. Chueh, "Synthesis of Si nanopyramids at SiO_x/Si interface for enhancing electroluminescence of Si-rich SiO_x," *Appl. Phys. Lett.*, vol. 89, no. 9, pp. 093126-1–093126-3, Aug. 2006.
[45] H. P. Maruska and D. A. Stevenson, "Mechanism of light production in metal-insulator-semiconductor diodes; GaN:Mg violet light-emitting diodes," *Solid State Electron.*, vol. 17, no. 11, pp. 1171–1179, Nov. 1974.